Available online at www.sciencedirect.com
ScienceDirect
Journal of the Mechanics and Physics of Solids
55 (2007) 1803–1822

JOURNAL OF THE MECHANICS AND PHYSICS OF SOLIDS

www.elsevier.com/locate/jmps

Concepts for structurally robust materials that combine low thermal expansion with high stiffness

Craig A. Steeves[a,*], Sergio L. dos Santos e Lucato[b], Ming He[a], Emilio Antinucci[a], John W. Hutchinson[c], Anthony G. Evans[a]

[a]*Department of Materials, University of California, Santa Barbara, CA 93106, USA*
[b]*Teledyne Scientific Co LLC, Thousand Oaks, CA 91360, USA*
[c]*Division of Engineering and Applied Science, Harvard University, Cambridge, MA 02138, USA*

Received 22 November 2006; received in revised form 23 February 2007; accepted 28 February 2007

Abstract

A family of robust stretch-dominated bimaterial lattices is introduced which combines low (or zero) thermal expansion with high stiffness, structural robustness over wide temperature ranges and manufacturing facility. This combination of properties is unavailable through any other material solution. The concept uses two constituents configured as adjoining sub-lattices. It accommodates the thermal expansion through rotation of the members of one sub-lattice. Moreover, the lattice exhibits large stiffness to weight because it is fully triangulated and does not rely on rotational resistance at the joints for structural rigidity. A wide range of constituents can be used to build the new lattices enabling many desirable properties to be incorporated, especially high strength and toughness. Examples of both planar and volumetric lattices are presented, and their thermo-mechanical properties derived. The results are verified by conducting experiments and finite element simulations on a lattice fabricated using aluminium and titanium alloy constituents.

Keywords: Thermomechanical processes; Structures; Thermal stress; Thermal expansion; Lattice materials

*Corresponding author. Tel.: +1 805 893 8374.
E-mail address: csteeves@engineering.ucsb.edu (C.A. Steeves).

0022-5096/$ - see front matter © 2007 Elsevier Ltd. All rights reserved.
doi:10.1016/j.jmps.2007.02.009

1. Introduction

Structural systems that experience large temperature changes are susceptible to extreme thermal stresses that activate failure by thermo-mechanical fatigue. To suppress such failures, the material should have a low thermal expansion coefficient, α, over a wide range of temperature. However, low α is not normally sufficient, but must be combined with adequate stiffness, strength and robustness (ductility and toughness) to support in-plane loads and bending moments. This combination of attributes cannot be found in any single-constituent material.

The available choices are apparent from material property maps, such as Fig. 1, which displays the known universe of robust materials in α/E (Young's modulus) space. Solids having low (or even negative) α exist, but all possess characteristics which limit their use in applications which demand robustness and durability over large temperature changes. Invar is robust, but has low expansion only between 0 and 100 °C (Fig. 2(a)). Zerodur (Schott Optics, 2006) has low expansion over a larger temperature range (Fig. 2a), but it is a glass ceramic and unsuitable for reliable load bearing structures. Composite materials incorporating carbon fibres have property combinations closest to the desired attributes. These fibres have very low axial α. When incorporated into a matrix, the ensuing materials combine low α with acceptable stiffness, but deficiencies have limited their application in demanding thermal scenarios. Specifically, when incorporated into an organic matrix, the large difference in the thermal expansion between the two constituents results in strains upon temperature cycling that cause matrix cracking and thermal fatigue. This deficiency is partially circumvented by using a carbon matrix. Such materials have low expansion up to 1500 °C (Fig. 2(b)), as well as

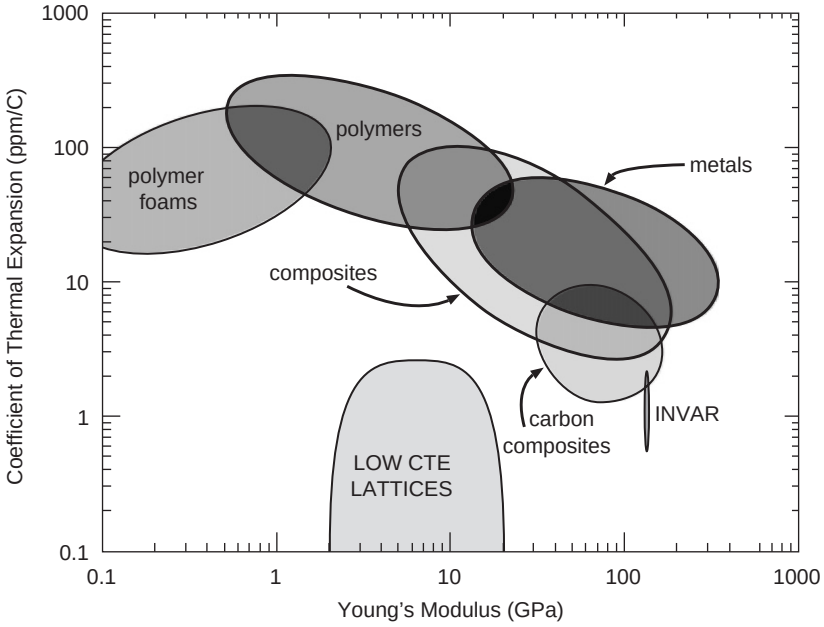

Fig. 1. The universe of available structurally robust materials (ceramics are not included), plotted in the space of stiffness and thermal expansion.

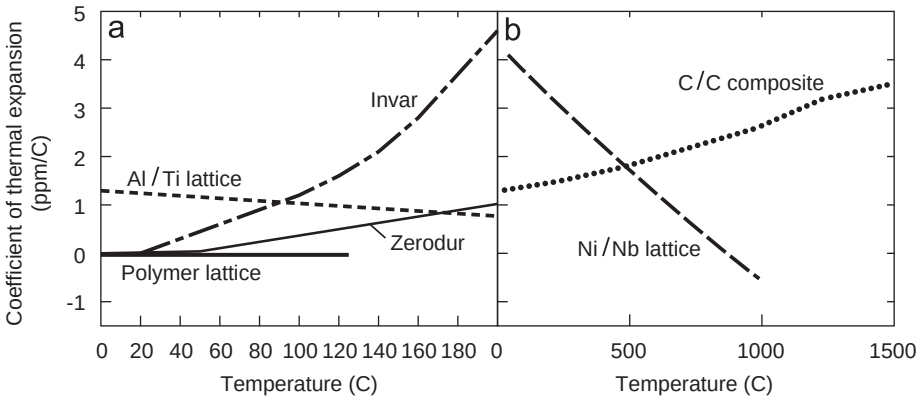

Fig. 2. The relationship between α and temperature for three solid materials: Invar, Zerodur and carbon–carbon composite; and three planar lattices composed of liquid crystal polymer (assuming that the anisotropy can be controlled) and polycarbonate with 8.65° skewness, titanium and aluminium with 24° skewness and niobium C-103 and Inconel 625 with 24° skewness.

reasonable stiffness. However, they experience severe oxidation at high temperatures, as well as robustness issues and manufacturing limitations.

The challenge to be pursued in this article is to begin with inherently robust constituents, either metallic or polymeric, which individually have large α. Topology concepts will then be used to generate a material having zero α over a large temperature range, combined with acceptable stiffness, strength and resistance to thermal fatigue. The approach to be pursued combines two disparate constituents to achieve properties outside the range attainable with each separately. That is, two constituents with widely different individual α will be combined with empty space to create a lattice material with low overall expansion. The original ideas for materials having these characteristics emerged from concepts proposed by Sigmund and Torquato (1996); Lakes (1996); Gibiansky and Torquato (1997); Sigmund and Torquato (1997) and, more recently, by Jefferson (2006). The topologies examined are summarized in Fig. 3. The bimaterial lattices presented in Fig. 3(a) (Lakes, 1996) and Fig. 3(c) (Jefferson, 2006) can be designed to have zero expansion, but both have low stiffness and strength because of the bending of one of the sub-lattices upon mechanical loading (that in black in Fig. 3(c)). This stiffness deficiency is obviated by the Sigmund and Torquato (1996) design (Fig. 3(b)), obtained by optimizing for combined zero expansion and maximum biaxial stiffness. The limitations of this material are that it is geometrically too complex for manufacturing and has only modest in-plane uniaxial stiffness. The goal here is to devise zero expansion lattices with topologies amenable to manufacturing that are stretch- (not bending-) dominated upon mechanical loading, enabling them achieve zero α while being relatively stiff and strong and resistant to thermal fatigue. The rules governing stretch-dominated structures have been elucidated by Gibson and Ashby (1997) and Deshpande et al. (2001b). Most notably, stretch-dominated structures have stiffness that scales linearly with relative density, $\bar{\rho}$, whereas their bending-dominated analogs have stiffness which scales with $\bar{\rho}^3$ for planar structures and with $\bar{\rho}^2$ for volumetric structures (Gibson and Ashby, 1997). Consequently, at the relative densities of interest, $0.1 \leqslant \bar{\rho} \leqslant 0.5$, the stretch-dominated designs have at least a factor 2–10 larger stiffness.

A preview of these concepts gives further context (Fig. 2). In the temperature range 0–300 °C (Fig. 2(a)), near-zero average α can be obtained with an all-metallic lattice that

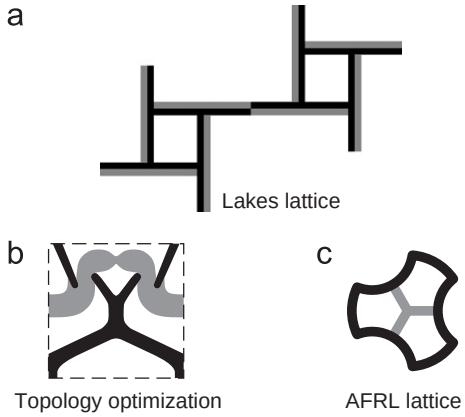

Fig. 3. Unit cells of planar lattices. (a) The Lakes configuration for arbitrary thermal expansion (Lakes, 1996). (b) A high-stiffness, zero thermal expansion lattice calculated using a topology optimization code (Sigmund and Torquato, 1996). (c) A low thermal expansion lattice proposed by Jefferson (2006). For each of these bimaterial lattices, the black constituent has a low coefficient of thermal expansion, while the grey constituent has a high coefficient of thermal expansion.

combines aluminium and titanium alloys, as well as an all-polymeric lattice that combines polycarbonate with liquid crystal polymer. Over a wider temperature range, 0–1000 °C (Fig. 2(b)), the new concept can realize near-zero average α with another all-metallic system that combines nickel and niobium alloys. The only competition is a carbon/carbon composite having the aforementioned limitations. To validate the concept and to demonstrate that these new materials can be manufactured in a practical manner, a lattice made from commercial aluminium and titanium alloys has been produced and tested.

The article is organized in the following manner: stretch-dominated planar lattices are devised that combine low α with high stiffness. The mechanics governing the thermal expansion and the stiffness are presented for pin-jointed lattices with slender members. It will be shown that these lattices can be designed to achieve zero thermal expansion coefficient, but also have stiffness close to the theoretical bounds. Next, to validate the theory, thermal expansion measurements are presented for a pinned planar lattice made from aluminium and titanium alloys. Additional validation is provided by finite element analysis of a bonded system. This same analysis is used to ascertain stresses induced around the bimaterial nodes during a temperature excursion to ensure that the lattice concept provides adequate resistance to thermal fatigue. Finally, the extension of the concept to a volumetric lattice is examined and the effective properties of these new materials are situated with respect to the universe of available materials.

2. Properties of stretch-dominated planar lattices

2.1. Topology

The following features characterize a family of planar lattices which combines low expansion with good strength and stiffness:

(i) It must incorporate at least two constituents with different α. Constituent 1 with the lower value, α_1, forms a continuous periodic lattice network composed of identical

polyhedral unit cells, configured as skewed versions of regular polyhedra. The skewness is essential to the attainment of zero expansion. Constituent 2, having the larger expansion, α_2, is arranged as discontinuous polyhedra contained within the unit cells of constituent 1. The polydedron of constituent 2 has the same number of vertices and sides as the unskewed analogue of the polyhedron of constituent 1.

(ii) The periodic structure contains two categories of nodes: (a) lattice nodes at which the unit cells of constituent 1 are connected and (b) expansion nodes where constituent 2 is connected to constituent 1.

(iii) The lattice must be fully triangulated within each unit cell so that the structure is stretch-dominated.

(iv) The topology should enable the length changes to be accommodated by a rotation (angle change) at the nodes, when pin-jointed. Such configurations provide high stiffness and strength. Structures with these characteristics based upon equilateral triangles, squares and hexagons are shown in Fig. 4.

We note that while the structural performance of the lattice is dependent upon the particular configuration of the constituent 2 component, the thermal behaviour is not; provided that constituent 2 is isotropic and simply connected, the overall lattice thermal properties depend only upon the configuration of the type 1 component and the location of the expansion nodes.

The examples to be evaluated are planar periodic lattices based upon an equilateral triangle (Fig. 5), which have isotropic planar thermal expansion and stiffness. From a thermal expansion perspective, this triangle can be open or solid. Members of constituent 1 have modulus, density and undeformed length denoted by E_1, ρ_1 and ℓ_1, respectively. The corresponding quantities for the members of constituent 2 are: E_2, ρ_2 and ℓ_2. The member cross-sections are solid and have areas A_1 and A_2. The overall geometry is determined by the length of the unit cell, L, and the skewness from an equilateral triangle, θ; see Fig. 5. With these geometric parameters, the undeformed lengths of the constituent members are

$$\ell_1 = \frac{L}{2\cos\theta}, \quad \ell_2 = \frac{L}{2}(1+\sqrt{3}\tan\theta) \tag{1}$$

such that

$$\mathrm{d}\ell_1 = \frac{\ell_1\,\mathrm{d}L}{L} + \frac{L\sin\theta\,\mathrm{d}\theta}{2\cos^2\theta}, \quad \mathrm{d}\ell_2 = \frac{\ell_2\,\mathrm{d}L}{L} + \frac{\sqrt{3}L\,\mathrm{d}\theta}{2\cos^2\theta}. \tag{2}$$

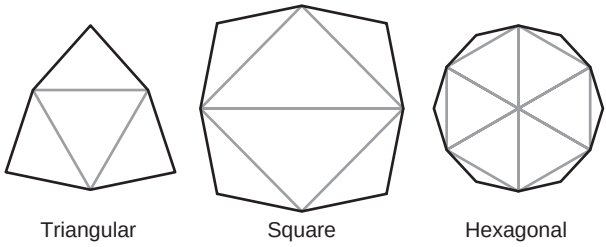

Fig. 4. Unit cells of planar lattices which are stretch-dominated and which can have low or zero net thermal expansion. The grey constituent has high α while the black constituent has low α.

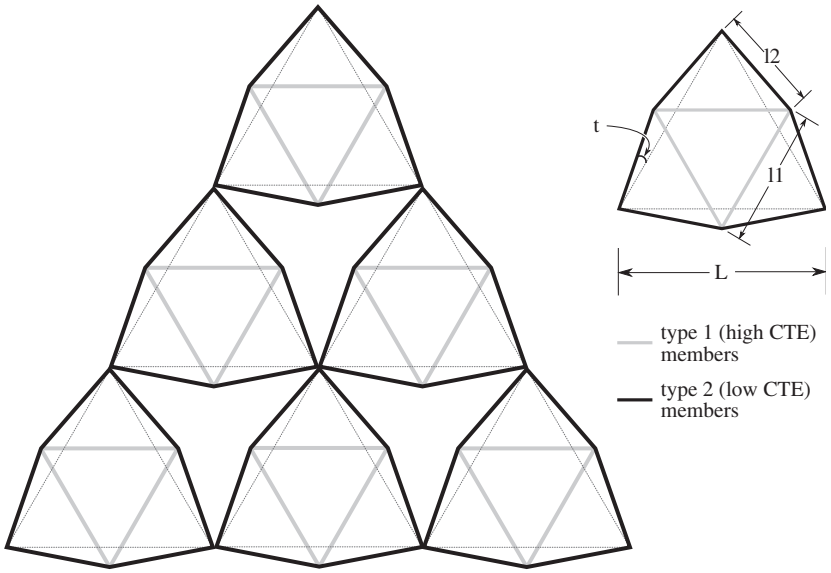

Fig. 5. A periodic planar lattice with a low net coefficient of thermal expansion. The grey constituent has high α while the black constituent has low α.

2.2. Thermal expansion

For homogeneous temperature changes, these lattices are isotropic in-plane. The lattice has thermal expansion $\bar{\alpha}$ defined such that an increment in temperature $\mathrm{d}T$ causes a length change $\mathrm{d}L = \bar{\alpha} L\,\mathrm{d}T$. When the lattice is pin-jointed, absent external stress, the members exhibit length changes $\mathrm{d}\ell_1 = \alpha_1 \ell_1 \mathrm{d}T$ and $\mathrm{d}\ell_2 = \alpha_2 \ell_2\,\mathrm{d}T$. The expansion coefficient is thus

$$\frac{\bar{\alpha}}{\alpha_1} = \frac{1 - \frac{1}{2}(\alpha_2/\alpha_1)\sin(2\theta)\left(\frac{1}{\sqrt{3}} + \tan\theta\right)}{1 - \frac{1}{2}\sin(2\theta)\left(\frac{1}{\sqrt{3}} + \tan\theta\right)}. \tag{3}$$

This relation is plotted in Fig. 6. It is apparent that the lattice has zero net thermal expansion within a realizable window of skewness, θ, and thermal expansion ratio, $\Sigma = \alpha_2/\alpha_1$. Specifically, when $\Sigma \approx 2.5$, zero thermal expansion emerges for skewness $\theta \approx 25^\circ$. It is important to note that the thermal expansion behaviour is a function only of the geometry of the lattice composed of constituent 1 and the locations of the expansion nodes; that is, the configuration of constituent 2 has no effect on the thermal behaviour of the lattice provided that constituent 2 expands isotropically. The structural behaviour of the lattice is, of course, dependent upon the configuration of constituent 2.

When the joints are pinned, no internal stresses are induced by a homogeneous temperature change. When bonded, they resist rotation and the members bend, generating internal stresses during thermal expansion. Finite element models have been created to assess their magnitude, as discussed below.

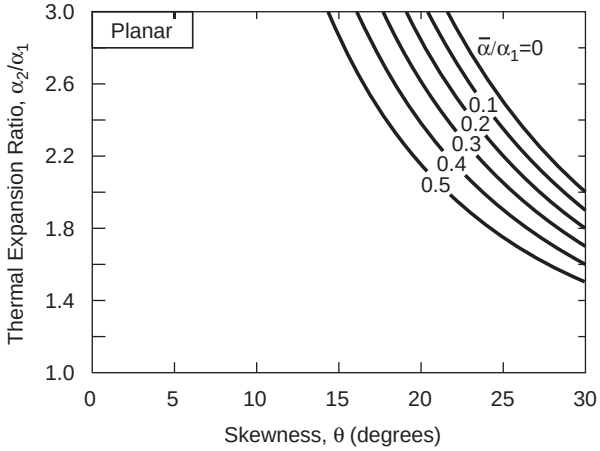

Fig. 6. Contours of normalized net thermal expansion coefficient $\bar{\alpha}$ of the planar lattice for a range of skewness.

2.3. Stiffness

Biaxial stiffness. The lattice is isotropic in-plane with biaxial stretching stiffness:

$$N_b = S_b \bar{\varepsilon}, \tag{4}$$

where N_b is the average force per unit length imposed on the structure in equibiaxial tension and $\bar{\varepsilon}$ is the resulting average strain ($\bar{\varepsilon}_{11} = \bar{\varepsilon}_{22} = \bar{\varepsilon}$). When pin-jointed, the forces F in the members are

$$F_1 = \frac{N_b L}{2\cos(\pi/6+\theta)}, \quad F_2 = -\frac{N_b L \sin\theta}{\sqrt{3}\cos(\pi/6+\theta)}. \tag{5}$$

Using (2) with $\varepsilon_1 = \mathrm{d}\ell_1/\ell_1 = F_1/E_1A_1$ and $\varepsilon_2 = \mathrm{d}\ell_2/\ell_2 = F_2/E_2A_2$, the strain becomes

$$\bar{\varepsilon} = \left(\frac{F_1}{E_1A_1} - \frac{2\sin\theta\sin(\pi/6+\theta)}{\sqrt{3}}\frac{F_2}{E_2A_2}\right) \Big/ \left(1 - \frac{2\sin\theta\sin(\pi/6+\theta)}{\sqrt{3}}\right). \tag{6}$$

Setting $Q = E_2A_2/E_1A_1$ and using (5) and definition (4), the structural stiffness in equibiaxial loading is

$$S_b = \frac{E_2A_2}{L}\frac{\cos(\pi/6+\theta)(3-2\sqrt{3}\sin\theta\sin(\pi/6+\theta))}{3Q+2\sin^2\theta\sin(\pi/6+\theta)}. \tag{7}$$

The structural efficiency, Π, under biaxial loading can be ascertained from (7) upon noting that the mass M per unit area of the lattice is

$$M = \frac{6\rho_1\ell_1A_1 + 3\rho_2\ell_2A_2}{\sqrt{3}L^2/2}, \tag{8}$$

such that

$$\Pi \equiv \frac{S_b\rho_1}{ME_1} = \frac{Q\cos\theta\cos(\pi/6+\theta)(3-2\sqrt{3}\sin\theta\sin(\pi/6+\theta))}{\sqrt{3}(3Q+4\sin^2\theta\sin(\pi/6+\theta))(1+(\rho_2E_1/\rho_1E_2)Q\sin(\pi/6+\theta))}. \tag{9}$$

This is plotted in Fig. 7(a) for $\rho_2 E_1/\rho_1 E_2 = 1$. To give context, the maximum possible structural efficiency, which arises for a triangulated lattice (skewness $\theta = 0^\circ$ and $A_2 = 0$), is $\Pi_{\max} = \frac{1}{2}$. Even for large skewness ($\theta \to 30^\circ$), the lattice retains 10% of $\Pi_{\max}$.

Uniaxial stiffness. When loaded uniaxially, most pin-jointed lattices (such as Fig. 3(c)) have internal mechanisms, with stiffness reliant on the bending and rotational resistance of the members and joints. In the new configuration, *loads are carried exclusively by stretching or compressing the lattice members*. The uniaxial stretching stiffness, S_u, is defined by $N_u = S_u \bar{\varepsilon}$, where N_u is the uniaxial force per length acting in any direction and $\bar{\varepsilon}$ is the associated overall strain in that direction. The expressions arising from the determination of the uniaxial stiffness are cumbersome, and hence are not presented here. Symmetries consistent with the solution periodicities are imposed on the unit of the lattice used in carrying out the calculation. The ensuing structural efficiencies are plotted in Fig. 7(b) and compared with the maximum for the triangulated lattice, $\Pi_{\max} = \frac{1}{3}$. Again, the lattice retains 15% of its maximum efficiency at large skewness.

In summary, this pin-jointed, planar lattice has the characteristic that, while realizing low or zero net expansion, it exhibits excellent stiffness in both biaxial and uniaxial loading.

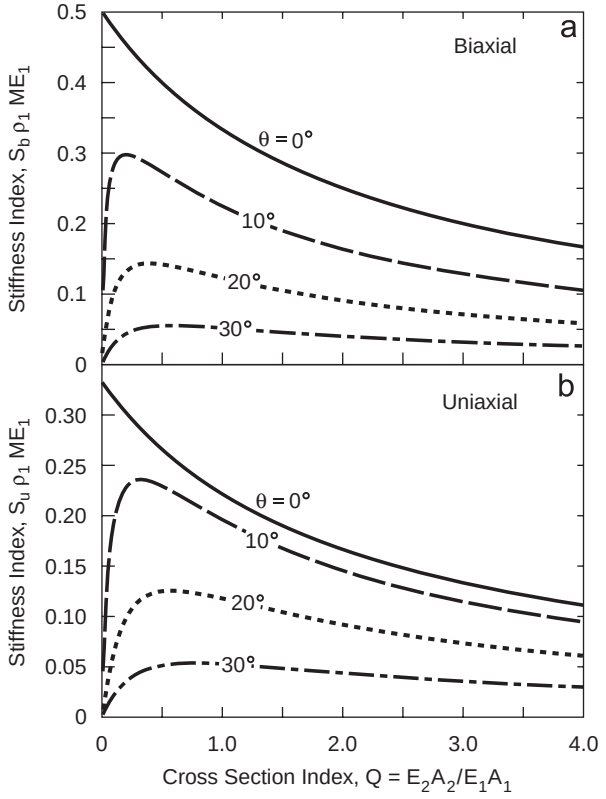

Fig. 7. Dimensionless stiffness for the triangular grid lattice for $\rho_1 E_2/\rho_2 E_1 = 1$. (a) Structural efficiency under biaxial loading, where a triangular grid ($\theta = 0, A_2 = 0$) is optimally stiff with $S_b \rho_1/ME_1 = \frac{1}{2}$. (b) Structural efficiency under uniaxial loading, where a triangular grid ($\theta = 0, A_2 = 0$) is optimally stiff with $S_u \rho_1/ME_1 = \frac{1}{3}$.

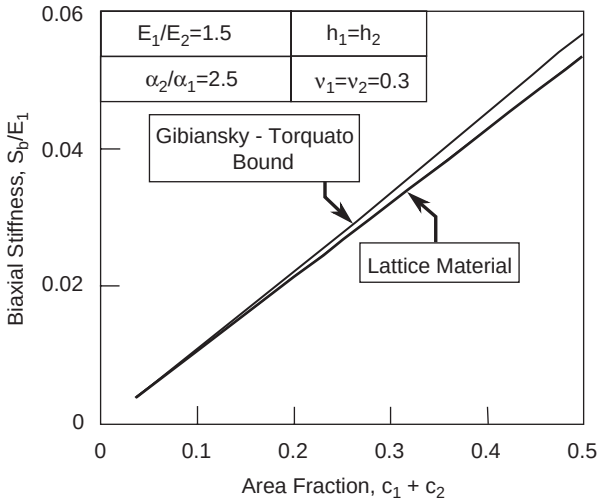

Fig. 8. For materials with $\bar{\alpha} = 0$, an example comparing the biaxial modulus, S_b, of the planar lattice material with the Gibianksy–Torquato upper bound over a range of the area fraction occupied by the two material phases. The curve for the lattice material is computed using (3) and (7) for the pin-jointed lattice.

2.4. Comparison with the Gibiansky–Torquato bound on biaxial stiffness

Gibiansky and Torquato (1997) have obtained the tightest bounds on the coefficient of thermal expansion of isotropic planar, three-phase systems when the overall in-plane biaxial modulus, S_b, is prescribed. These bounds can be applied to the present lattice material by identifying the respective members with phases 1 and 2 and invoking rectangular cross-sections with unit thickness and in-plane widths, h_1 and h_2. The member area fractions, $c_1 = 6h_1/3L\cos\theta$ and $c_2 = 3h_2(1 + 3\tan\theta)/L$, as well as E_1, ν_1, α_1, E_2, ν_2 and α_2 are prescribed. The third phase is the void space having area fraction, $c_3 = 1 - c_1 - c_2$. As illustrated by Sigmund and Torquato (1997), for materials with $\bar{\alpha}$ prescribed to be zero, the lower of the two Gibiansky–Torquato bounds provides an upper bound on S_b.

The biaxial modulus, S_b, computed for the pin-jointed lattice with the ratio of the two phase area fractions fixed ($h_1 = h_2$), plotted in Fig. 8, is compared with the upper bound calculated with the formulae provided by Sigmund and Torquato (1997).[1] While the results at larger area fractions ($c_1 + c_2$) become suspect (because the formulas (3) and (7) tacitly assume slender members), the closeness of the bound at low area fractions suggests the present lattice material may be optimal. (Note that while the result for the present lattice in Fig. 8 does not depend on the Poisson ratios, ν_1 and ν_2, the bound does. Nevertheless, by computing results for various combinations of ν_1 and ν_2, we have established that the bound is weakly dependent on the Poisson ratios.)

We have performed similar comparisons for the $\bar{\alpha} = 0$ planar materials considered by Sigmund and Torquato (1997), using $E_2/E_1 = 1$, $\alpha_2/\alpha_1 = 10$, $\nu_1 = \nu_2 = 0.3$ and $c_1 = c_2$. In their assessment, topology optimization was used to generate an isotropic planar material

[1]The formulae listed by Sigmund and Torquato (1997), while fairly complicated, are misprint-free. We have reproduced their figures with the formulae they provide.

that maximizes S_b for the case $c_1 = c_2 = 0.25$ (the result is shown here in Fig. 3(b)). Their material had biaxial stiffness 15% below the Gibiansky–Torquato bound, comparable to the present lattice material. However, their material has in-plane Poisson ratio $\bar{\nu} = 0.54$, implying a uniaxial to biaxial stiffness ratio, $S_u/S_b = 0.46$. The present lattice material has $S_u/S_b \cong 1$ and is thus *about twice as stiff in uniaxial stressing*. In a very recent development, Sigmund (2006) has used the lattice in Fig. 5 with $c_1 = c_2 = 0.25$ as a starting shape in the Sigmund–Torquato optimization program and performed search computations for an isotropic material with $\bar{\alpha} = 0$ for two different cases: maximization of S_b, and maximization of S_u. In both cases, the search produced a lattice-type structure similar to that in Fig. 5 having S_b close to the bound *as well as* high values of S_u. An interesting feature of this latest topology optimization is that the ends of members 2 (but not members 1) taper to a small section suggesting that these ends are effectively pinned in the optimal structure.

3. Experimental validation for the planar lattice

In this section, the practicality of a planar lattice design made from robust, all-metallic constituents is explored and combined with a preliminary validation of the thermal expansion characteristics. For this purpose, two constituent materials are selected having thermal expansion ratio in the range, $\Sigma \equiv \alpha_2/\alpha_1 = 2 \to 3$ (Fig. 6). A combination of a titanium alloy (Ti–6Al–4V) as constituent 1 with an aluminium alloy (7075-T6) as constituent 2 satisfies this requirement. Over the range 20 –250 °C, the average thermal expansions are 10.3 and 25.6 ppm/C for the titanium and aluminium alloys, respectively, giving an overall average $\Sigma = 2.5$ (Table 1). For this assessment, solid triangles of aluminium were used for ease of manufacturing and because, thermally, the solid is equivalent to a triangular truss. Predictions of the influence of skewness on the lattice thermal expansion for this material combination (Fig. 9) guide the experimental design. Note that the critical skewness giving zero average thermal expansion is, $\theta_{zero} \approx 25°$. Unit cells have been made with both bonded and pinned joints (Fig. 10). Those with the bonded joints have skewness, $\theta = \theta_{zero}$. The specimens were manufactured using protocols established for lattice materials (Wadley et al., 2003); namely, by laser cutting from sheets of the constituent materials, then assembled and finally bonded by either brazing or laser welding.

Table 1
Material properties for the titanium and aluminium alloys used in the numerical simulations, including the variation of yield strength and thermal expansion with temperature

Material	Young's modulus (GPa)	Yield strength		Thermal expansion	
		σ_Y (MPa)	T(°C)	α (ppm/C)	T(°C)
Al alloy	70	434	20	24.0	0
7075-T6		391	200		
		339	300	27.2	300
Ti alloy	110	1100	20	9.9	20
Ti–6Al–4V		858	300	10.6	300

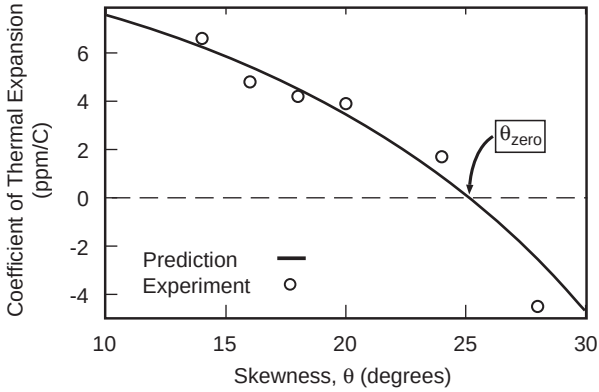

Fig. 9. Predicted curve and experimental results for titanium–aluminium planar lattices with a range of skewness.

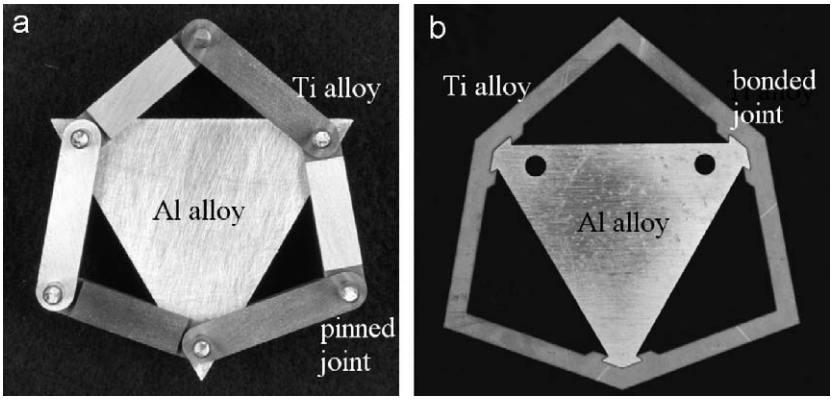

Fig. 10. (a) A pinned planar experimental specimen composed of titanium 6Al–4V and aluminium 7075-T6 with relative density $\bar{\rho} \approx 0.25$. (b) An example of a bonded unit cell of the same materials; $\bar{\rho} \approx 0.12$. The relative densities are calculated based upon the geometry of the constituent 1 members using equation (10).

The configuration with the pinned joints has been used to validate Fig. 9 by performing tests over the skewness range $14^\circ \leqslant \theta \leqslant 28^\circ$. The specimens were heated slowly between ambient and 250 °C in a furnace and allowed to air cool. The temperature was determined using thermocouples located on both the aluminium and the titanium, while the displacement between adjacent lattice nodes was measured with a scanning laser extensometer. Two types of experiment were conducted. (i) The average values of thermal expansion coefficient for the lattice over this temperature range were determined from the recorded data and plotted in Fig. 9. (ii) Since the thermal expansion coefficients of both alloys are temperature dependent (Table 1), the variation of $\bar{\alpha}$ with temperature was measured for fixed skewness, using values close to θ_{zero} (both 20° and 24°). The results are plotted in Fig. 11, along with the predictions. The correspondence between both sets of measurements and the predictions affirms the analysis and verifies the existence of all-metallic lattices having near zero thermal expansion over an appreciable range of temperature.

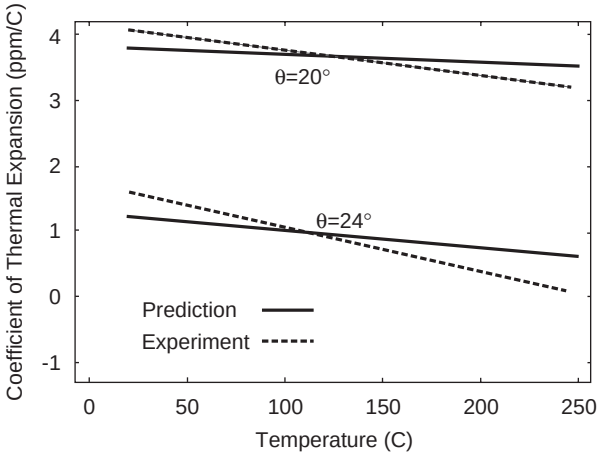

Fig. 11. The variation of $\bar{\alpha}$ for $\theta = 20^\circ$ and 24° planar lattices. The theoretical predictions are shown as solid lines while the experimental results are the dotted lines.

4. Stress concentrations at bonded joints

Actual structures typically use bonded attachments made by brazing or electron beam welding (Wadley et al., 2003). Bonded connections generate a rotational resistance at the joints and induce bending of the lattice members. The moment resistance of a member is a function of the slenderness ratio r/L, which, for square members and when $A_1 = A_2$, is related to the relative density $\bar{\rho}$ through

$$\bar{\rho} = \frac{r}{L}\frac{2(1+\cos\theta+\sqrt{3}\sin\theta)}{\cos\theta}. \tag{10}$$

Here the relative density is expressed in terms of relative areas. The calculation of the uniaxial structural efficiency (Appendix A, Fig. 14(b)) reveals that at skewness close to θ_{zero} the stiffness can increase markedly as the members become stubbier ($r/L > 0.04$). This increase in stiffness has two consequences. (i) The requisite skewness angle for zero expansion deviates from θ_{zero}. (ii) Bending stresses are induced that might cause yielding. Additionally, at the nodes, the thermal misfit between the constituents produces stress concentrations that might also induce yielding.

To examine these issues, finite element calculations have been performed for the lattice depicted on Fig. 12, chosen to have skewness angle close to θ_{zero}. The $\frac{1}{6}$ unit cell has been used. Note that, to fit the cells together, a section AC is required having inclination differing from that along DC. Periodic boundary conditions are imposed as follows (see Fig. 12). Point E is fixed to avoid rigid body displacements. The segments EF and AB are prohibited from displacing in the x-direction but can displace vertically. The section ED is prohibited from displacing along its normal, but elongation along its length is allowed so that D can displace outward and upward ($u_x \sin 60^\circ = u_y \cos 60^\circ$). The segment AC displaces uniformly along its normal, with displacement in the y-direction compatible with the displacement of A. The segment can also elongate. Subject to these boundary conditions, calculations are conducted with the finite element code ABAQUS (HKS, 2005),

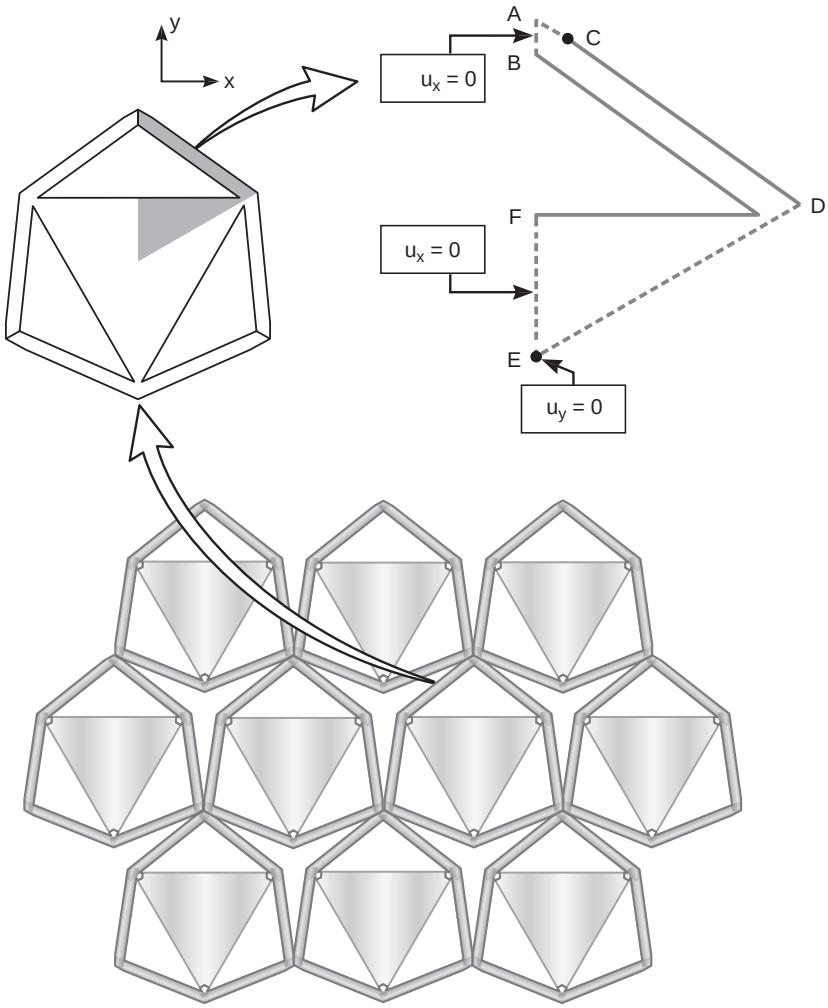

Fig. 12. The bonded planar lattice used in the finite element simulations. Due to the symmetries of the lattice, $\frac{1}{6}$ of a unit cell is modeled, shown with the imposed boundary conditions.

using the material properties from Table 1, for two values of skewness, $\theta = 20^\circ, 24^\circ$. A typical mesh includes about 1000 8-node generalized plane strain elements.

For all temperature variations within the operating ranges, the stresses induced in the members during a thermal excursion are found to be extremely small, except for those concentrated at bonded interfaces. A preliminary step in the analysis adjusts the contact length AC of the joints (Fig. 12) to find geometries that minimize the mismatch. Contours of the local Mises stresses at maximum temperature are shown in Fig. 13. For the design shown, the ratio of the Mises stress to the yield strength, which is largest in the aluminium alloy, remains below unity everywhere. Since both materials remain elastic, the thermal expansion of the lattice is found to be invariant with thermal cycling.

For different material combinations or larger thermal excursions, the yield strength of one or both of the materials may be surpassed, causing local plastic flow. The plastic

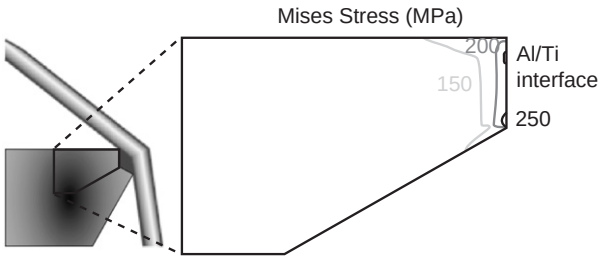

Fig. 13. The local Mises stresses at the aluminium/titanium interface in the lattice shown in Fig. 12 due to a temperature increase from 20–250 °C.

deformation will redistribute the stresses (analogous to stress effects at notches; see Hult and McClintock, 1957) and that, in some cases, shakedown will occur (Bree, 1967). To ascertain the associated limitations, these phenomena must be explored further, both experimentally and with finite element simulations.

5. Situating the lattices within the universe of available materials

The low α lattices provide a combination of characteristics previously unattainable: good stiffness and strength in an easily manufactured geometry with low (or zero) net thermal expansion over large temperature ranges. Moreover, by extending the concept to a volumetric lattice (see Appendix B), a material can be envisaged that occupies a large gap in stiffness–thermal expansion space (see Fig. 1). (Note that the low expansion of Invar is restricted to a small range of operational temperatures.) Since the new lattices can be constructed using metals (or plastics), it is possible to build robust materials with unprecedented thermo-mechanical properties.

Some specifics have been illustrated by Fig. 2 using two metallic and one polymer lattice, as well as one low α ceramic, one metal and one composite. Each curve is terminated at the maximum use temperature. In general, α for solid materials increases with temperature, while α for the lattices declines with temperature. As a consequence, the skewness of the lattice structure can be chosen to provide zero net expansion over the desired temperature range. It is also significant that, by choosing the correct combination of materials and skewness, lattice structures can be designed to perform better than all other materials over any temperature range for which the constituents retain structural stiffness.

Finally, other unusual combinations of properties can be achieved. For example, a material with low thermal expansion and high thermal or electrical conductivity could be designed. Again, this combination of properties is unattainable using conventional materials. Moreover, negative α materials can be created, as well as those with very high α. The primary restriction is finding two materials with sufficiently different α, which are mechanically and chemically compatible and can be joined effectively.

6. Concluding remarks

A family of lattices with low thermal expansion and high structural stiffness has been introduced. The thermal expansion of the members is accommodated by rotations

at the nodes. The high structural stiffness arises because the mechanical response of the lattices is dominated by stretching, rather than bending. By appropriate selection of the constituents and the skewness θ, a lattice with any desired α can be created. This permits the design of a coefficient of thermal expansion that precisely matches the application. Importantly, because these lattices can be fabricated from a wide range of constituents, they can be designed to exhibit high strength and toughness. Not only can the lattices be designed for zero expansion, they also have biaxial and uniaxial stiffness close to the theoretical bounds and are thus superior to all previously known concepts. Extension of these lattices into three dimensions is straightforward, involving a skewed tetrahedral unit cell containing a regular octahedron (see Appendix B).

An experimental program has been initiated to validate the performance of these lattices. Pinned planar lattices with a range of θ and Σ have been constructed and are being subjected to large temperature excursions; preliminary results have been presented here. To assess the effects of rigid connections, test pieces with rigidly bonded joints are being tested. These tests will determine the extent of plasticity due to thermal mismatch and member bending, as well as the net geometric changes due to thermal cycling. The experimental program will be coupled with a series of finite element calculations to determine geometries which exhibit shakedown rather than ratcheting.

In summary, the lattice materials introduced here provide the unique combination of low thermal expansion with high stiffness in an easily manufacturable, yet structurally robust, geometry. Single-constituent materials may have low α, but are either brittle (ceramics), have a narrow range of low expansion (Invar) or have manufacturing or usage limitations (carbon/carbon composites).

Acknowledgements

The funding for this research was provided by the Office of Naval Research through a MURI program on Revolutionary Materials for Hypersonic Flight (Contract No. N00014-05-1-0439).

Appendix A. Properties of bonded planar lattices

Connecting the lattice members with joints capable of carrying moments, either by welding or another form of bonding, changes the thermal and mechanical properties of the lattice. The members have second moments: $I_1 = A_1 r_1^2$ and $I_2 = A_2 r_2^2$ and slenderness ratios r_1/L and r_2/L.

A.1. Thermal expansion

With the parameter $C_1 = A_1 \ell_1 / I_1$ representing the bending stiffness of the members, the normalized $\bar{\alpha}$ of the bonded planar lattice is

$$\frac{\bar{\alpha}}{\alpha_1} = 1 - \frac{(C_1 \tan\theta - 12\sqrt{3})\,(\cos\theta + \sqrt{3}\sin\theta)(\alpha_2/\alpha_1 - 1)}{C_1(\sqrt{3}\cos\theta - \sin\theta) + 12(\sqrt{3} + 2E_1A_1/E_2A_2)(\cos\theta + \sqrt{3}\sin\theta)} \tag{A.1}$$

which in the limit as the slenderness ratio $r_1/L \to 0$ reduces to the result for pinned lattices. Sample results for this calculation are shown in Fig. 14(a). The effect of bonding the joints is to increase $\bar{\alpha}$ above that expected for pinned joints comprising the same constituent materials and geometry. Consequently, θ_{zero} for the pinned lattice must be reassessed when the joints are bonded to assure an accurate choice.

A.2. Stiffness

The uniaxial stiffness of the bonded planar lattice is dependent upon the bending stiffness of the constituent members, and can be determined by constructing the structural stiffness matrix. The stiffness matrix K is related to the force vector F and the deflection vector u through the relation $Ku = F$. Results for the bonded lattice loaded uniaxially are shown in Fig. 14(b). The stiffness calculation reduces to that of the pin-connected lattice when $I_1 = I_2 = 0$.

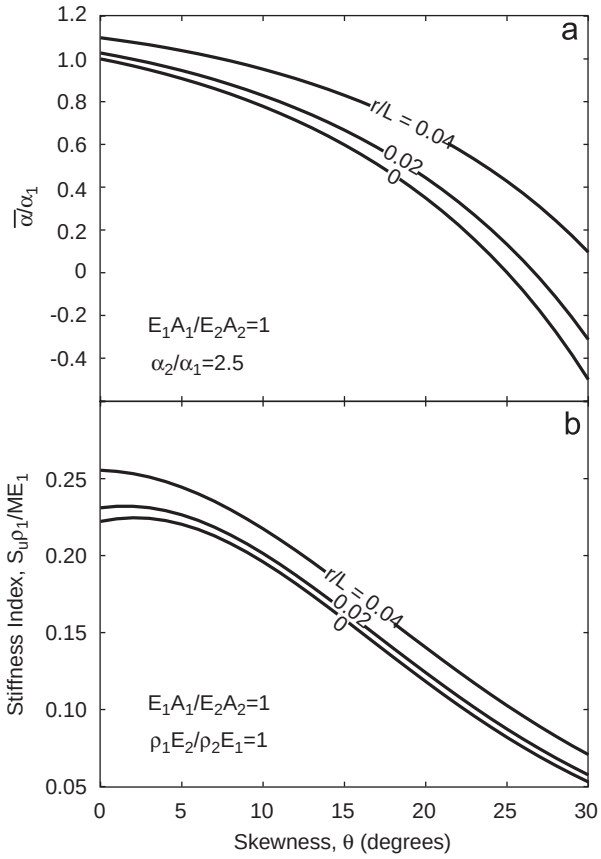

Fig. 14. (a) Normalized net coefficient of thermal expansion for the bonded planar lattice with $\alpha_2/\alpha_1 = 2.5$ and $E_1A_1/E_2A_2 = 1$ for a range of slenderness ratios (r/L) of the members; $r/L = 0$ is for the pinned structure. (b) Dimensionless uniaxial stiffness for the bonded planar lattice for $\rho_1E_2/\rho_2E_1 = 1$ and $E_1A_1/E_2A_2 = 1$. The lattice unit cell shown in Fig. 10(b) has $r/L = 0.02$.

Appendix B. Properties of stretch-dominated volumetric lattices

B.1. Topology

Three-dimensional periodic lattice structures comprise a skewed polyhedral solid of low-α constituent 1 connected to form a volumetric lattice in which each cell contains a high-α polyhedron of constituent 2. In contrast to the two-dimensional case, the polyhedron of constituent 2 has twice the number of sides as that for constituent 1. We describe an example based upon a skewed tetrahedron of constituent 1, containing an octahedron of constituent 2 (Fig. 15). The unit cell of this configuration contains four lattice nodes and six expansion nodes. The full lattice geometry has the same underlying structure as the octet (octahedron–tetrahedron) truss described by Fuller (1961), Deshpande et al. (2001a) and Christensen (2004) with the skewed tetrahedra of Fig. 15(b) replacing the regular tetrahedra of the octet truss. The length of the cell is L and the skewness, θ, is defined as the angle projected onto a plane between a regular tetrahedron and the constituent 1 lattice members. This definition of θ is chosen so that for both the planar and volumetric cases, $0^\circ \leqslant \theta < 30^\circ$, and is shown in Fig. 15(c). Given these definitions, the lengths of the two constituent members are

$$\ell_1 = \frac{L}{2}\left(1 + \frac{\tan^2\theta}{\cos^2 a}\right)^{1/2}, \quad \ell_2 = \frac{L}{2}\left(1 + \sqrt{3}\tan\theta\right), \tag{B.1}$$

where $a = \frac{1}{2}\tan^{-1}(2\sqrt{2})$.

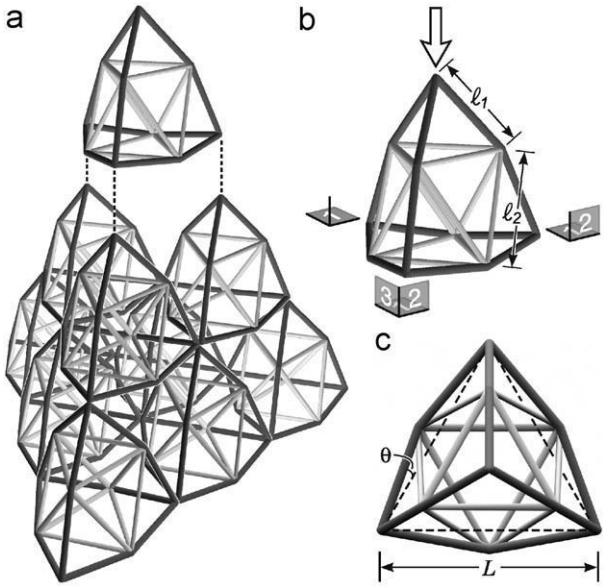

Fig. 15. A three-dimensional periodic lattice with a low coefficient of thermal expansion. The dark grey members of constituent 1 have low α while the light grey members of constituent 2 have high α. (a) The lattice structure, similar to an octet truss, and how the individual unit cells are connected. (b) The unit cell, and the loading configuration and constraints for the uniaxial stiffness. (c) A view normal to the plane of three lattice nodes showing the skewness θ and unit cell length L. Note that θ is defined by the projection of the constituent 1 members onto a plane.

B.2. Thermal expansion

For a homogeneous temperature change, the thermal expansion of the volumetric lattice is isotropic, and is defined such that an increment in temperature $\mathrm{d}T$ produces a length change $\mathrm{d}L = \bar{\alpha} L\,\mathrm{d}T$. Following the same procedure outlined above for the planar lattice, the net thermal expansion $\bar{\alpha}$ of the volumetric lattice is given by

$$\frac{\bar{\alpha}}{\alpha_1} = \frac{\sqrt{3}(\cos^2 a + \tan^2\theta) - (\alpha_2/\alpha_1)\,\tan\theta(1+\sqrt{3}\tan\theta)}{\sqrt{3}\cos^2 a - \tan\theta} \tag{B.2}$$

This relation is plotted in Fig. 16. Again, for realizable skewness, there is an opportunity to create structures with very small net thermal expansion. Comparison with Fig. 6 shows that the requirements for low $\bar{\alpha}$ volumetric structures are slightly less stringent than for the planar structures; that is, volumetric structures require lower skewness to attain equivalent α.

B.3. Stiffness

Hydrostatic stiffness. The hydrostatic stiffness S_h of the volumetric truss is defined by $N_\mathrm{h} = S_\mathrm{h}\bar{\varepsilon}$ where N_h is the hydrostatic stress and $\bar{\varepsilon}$ is defined as $\mathrm{d}L/L$:S_h *is three times the bulk modulus*. It is convenient to calculate the hydrostatic stiffness of the pin-jointed volumetric lattice using the method of virtual work. For an applied hydrostatic stress $N_\mathrm{h} = 2P/\sqrt{3}L^2$, the member forces in the constituent 1 and constituent 2 members are, respectively,

$$F_1 = \frac{P}{3\sin(b-c)}, \quad F_2 = -\frac{P}{3\sqrt{3}}\left(\frac{1}{\tan(b-c)} - \frac{1}{\tan(b)}\right), \tag{B.3}$$

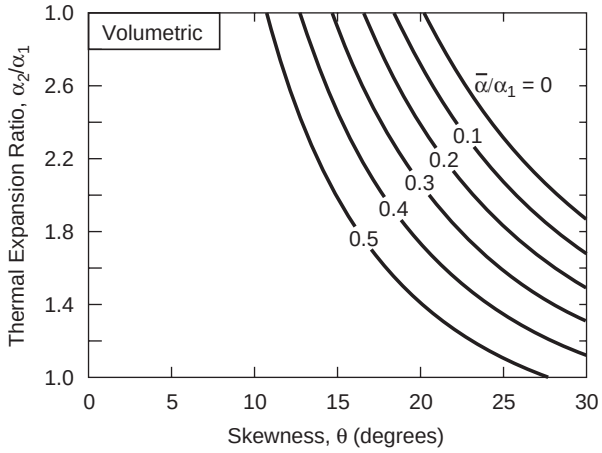

Fig. 16. Contours of normalized net thermal expansion coefficient $\bar{\alpha}$ of the volumetric lattice for a range of skewness.

where $b = \tan^{-1}\sqrt{2}$ and $c = \tan^{-1}(\tan\theta/\cos a)$. The displacement at each tetrahedral vertex is

$$u = \frac{3\ell_1 F_1 \delta F_1}{A_1 E_1 \delta P} + \frac{3\ell_2 F_2 \delta F_2}{A_2 E_2 \delta P}, \tag{B.4}$$

for virtual nodal forces δP which induce virtual member forces δF. The hydrostatic stiffness S_h is then given by

$$S_h = \frac{P}{\sqrt{2}Lu}. \tag{B.5}$$

The mass per unit volume of the unit cell is given by

$$M = \frac{12A_1\ell_1\rho_1 + 12A_2\ell_2\rho_2}{L^3/\sqrt{3}}. \tag{B.6}$$

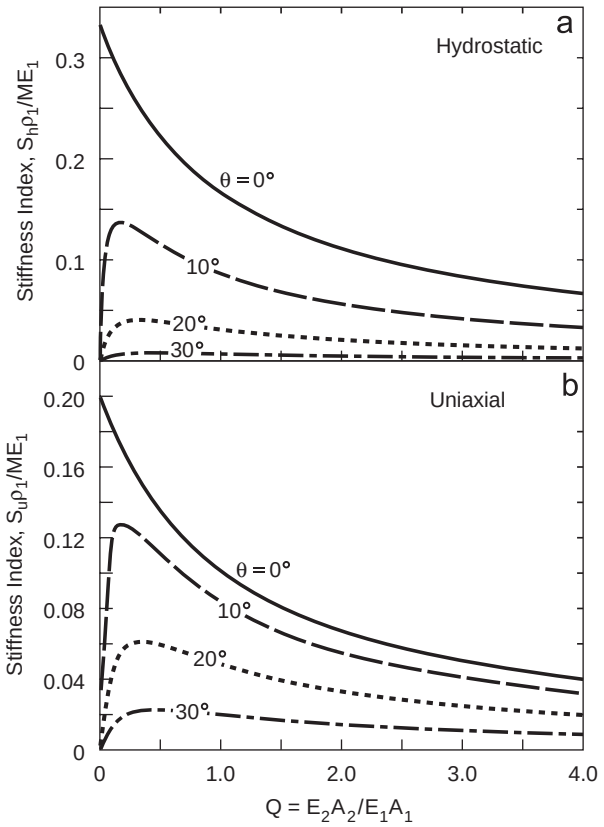

Fig. 17. The non-dimensional stiffness of the tetrahedral volumetric lattice when $\rho_1 E_2/\rho_2 E_1 = 1$. (a) Hydrostatic, where a tetrahedral grid ($\theta = 0, A_2 = 0$) is optimally stiff with $S_h\rho_1/ME_1 = \frac{1}{3}$. (b) Uniaxial, in a direction normal to a plane containing three lattice nodes, where a tetrahedral grid ($\theta = 0, A_2 = 0$) is optimally stiff with $S_u\rho_1/ME_1 = \frac{1}{5}$.

A plot of the structural efficiency, $\Pi = S_h \rho_1 / M E_1$, for a range of skewness (Fig. 17(a)), reveals that the structure retains approximately 5–10% of the maximum achievable efficiency, $\Pi_{max} = \frac{1}{3}$, found for a perfect tetrahedron ($\theta = 0$) of constituent 1 members.

Uniaxial stiffness. The pin-jointed volumetric lattice has the same cubic symmetry as the octet truss, and hence is not mechanically isotropic. The maximum stiffness occurs for loadings applied normal to a plane containing three of the lattice nodes (Deshpande et al., 2001a). The corresponding uniaxial stiffness for the low α volumetric lattice has been calculated by finite elements (using ABAQUS beam elements) for a structure idealized as a simply supported set of pin-connected truss members loaded at one tetrahedral vertex. Specifically, the unit cell is loaded at one lattice node in a direction normal to a plane containing the other three lattice nodes. The loaded node is permitted to displace freely, while the other three nodes are constrained in, respectively, one, two and three orthogonal directions (see Fig. 15(b)). These conditions reproduce the symmetries in the complete volume-filling lattice. The uniaxial modulus S_u calculated with this set of loads and boundary conditions *is equivalent to the overall Young's modulus in this direction*. The trends in uniaxial structural efficiency are plotted in Fig. 17(b). For a perfect tetrahedron ($\theta = 0$ and $A_2 = 0$) the maximum structural efficiency is $\Pi_{max} = \frac{1}{5}$, which duplicates the result of Deshpande et al. (2001a) for the octet truss without the members of constituent 2.

References

Bree, J., 1967. Elastic–plastic behaviour of thin tubes subjected to internal pressure and intermittent high-heat fluxes with applications to fast-nuclear-reactor fuel elements. J. Strain Anal. 2 (3), 226–238.

Christensen, R.M., 2004. The three-dimensional analog of the classical two-dimensional truss system. J. Appl. Mech. 71 (2), 285–287.

Deshpande, V.S., Ashby, M.F., Fleck, N.A., 2001a. Effective properties of the octet-truss lattice material. J. Mech. Phys. Solids 49 (8), 1747–1769.

Deshpande, V.S., Ashby, M.F., Fleck, N.A., 2001b. Foam topology: bending versus stretching dominated architectures. Acta Mater. 9 (6), 1035–1040.

Fuller, R.B., 1961. Octet truss. US Patent Serial No. 2986241.

Gibiansky, L.V., Torquato, S., 1997. Thermal expansion of isotropic multiphase composites and polycrystals. J. Mech. Phys. Solids 45 (7), 1223–1252.

Gibson, L.J., Ashby, M.F., 1997. Cellular Solids, second ed. Cambridge University Press, Cambridge.

HKS, 2005. ABAQUS/Standard User's Manual, 6.5 ed. HKS, Providence, RI.

Hult, J.A.H., McClintock, F.A., 1957. Elastic–plastic stress and strain distributions around sharp notches under repeated shear. In: Proceedings of the Ninth International Congress for Applied Mechanics, Brussels, pp. 51–58.

Jefferson, G., 2006. Private communication. Air Force Research Lab.

Lakes, R.S., 1996. Cellular solid structures with unbounded thermal expansion. J. Mater. Sci. Lett. 15 (6), 475–477.

Schott Optics, 2006. Tie-37: Thermal Expansion of ZERODUR Data Sheet. Schott optics. Duryea, PA, USA.

Sigmund, O., 2006. Private communication. Technical University of Denmark.

Sigmund, O., Torquato, S., 1996. Composites with extremal thermal expansion coefficients. Appl. Phys. Lett. 69 (21), 3203–3205.

Sigmund, O., Torquato, S., 1997. Design of materials with extreme thermal expansion using a three-phase topology optimization method. J. Mech. Phys. Solids 45 (6), 1037–1067.

Wadley, H.N.G., Fleck, N.A., Evans, A.G., 2003. Fabrication and structural performance of periodic cellular metal sandwich structures. Compos. Sci. Technol. 63 (16), 2331–2343.